Focal Depth Determination for Moderate and Small Earthquakes by Modeling Regional Depth Phases sPg, sPmP, and sPn

Chapter *in* Bulletin of the Seismological Society of America · February 2012

DOI: 10.1785/0120090103 · Source: InTech

1 author:

Shutian Ma
Carleton University
38 PUBLICATIONS **328** CITATIONS

SEE PROFILE

7

Focal Depth Determination for Moderate and Small Earthquakes by Modeling Regional Depth Phases *sPg*, *sPmP*, and *sPn*[*]

Shutian Ma
Carleton University
Canada

1. Introduction

Earthquake focal depth is a critical parameter for seismological research, seismotectonic study, seismic hazard assessment, and event discrimination. For most earthquakes with M_W ≥4.5, the focal depth can be estimated from the arrival times of the teleseismic depth phase *sP* (or *pP*) and its reference phase *P*. Many seismologists have studied how to detect and use teleseismic depth phases to estimate focal depth (e.g., Goldstein and Dodge, 1999). For smaller earthquakes, focal depths can be estimated jointly while being located with the arrival times of the *Pg* and *Sg* phases recorded at close stations. Because stations in a regional network are generally not dense enough to control focal depth, operators often use default focal depths for regional events.

If regional depth phases can be identified, an alternative solution for moderate and small earthquakes is to use regional depth phases to estimate focal depth. The *P* portion of regional waveform records contains three major parts: (1) the *P*-wave travels directly to the station; (2) the *P*- or *S*-wave travels upward to the surface in the source region, is reflected or converted at the surface and then travels downward to the Moho (or interfaces), is reflected or refracted there, and then travels upward to the station; and (3) the *P*-wave travels downward to the Moho (or interfaces), is reflected there and then travels upward to the station. One feature of *P*- and *S*-waves is that the amplitude of the *S*-wave radiated from the source is generally stronger than that of the *P*-wave by about five times (Aki and Richards, 1980) and the period of the *S*-wave is longer than that of the *P*-wave on the same record.

From this analysis we know that there are regional depth phases in the *P* portion of the record and the usable regional depth phases are (1) *sPg* (the *S*-wave travels upward to the surface, is converted to a *P*-wave at the critical angle, then the *P*-wave travels along or close the surface to the station), (2) *sPmP* (the *S*-wave travels upward to the surface, is converted to a *P*-wave, then the *P*-wave travels downward to the Moho, is reflected there and travels upward to the station; Langston *et al*., 2003), and (3) *sPn* (the *S*-wave travels upward to the surface, is converted to a *P*-wave, then the *P*-wave travels along the *Pn* path to the station;

[*] This chapter is adapted from the paper "Focal Depth Determination for Moderate and Small Earthquakes by Modeling Regional Depth Phases *sPg*, *sPmP*, and *sPn*", *Bull. Seism. Soc. Am.* **100,** 1073-1088

Zonno and Kind, 1984). Fig. 1 (Ma and Eaton, 2011) shows the sketch paths of these regional depth phases. Many scientists have studied regional depth phases to some extent (e.g., King, 1979; Helmberger and Engen, 1980; Langston, 1987, 1996; Mulder and Lamontagne, 1990; Zhao and Helmberger, 1991, 1993; Bock, 1993; Ebel, 1995; Bock *et al*., 1996; Zhu and Helmberger, 1997; Saikia, 2000; Saikia *et al*., 2001; Bent and Perry, 2002; Savage *et al*., 2003; Uski *et al*., 2003).

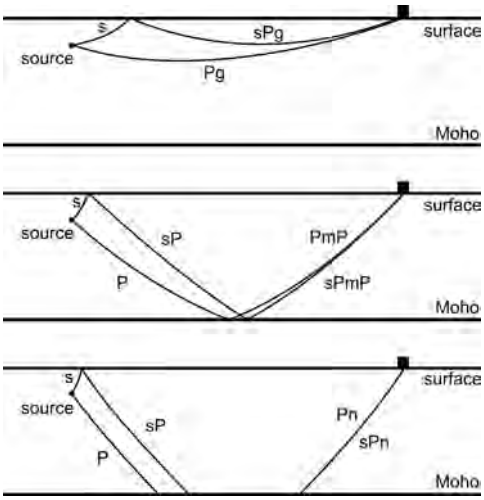

Fig. 1. Sketch figures for regional depth phase *sPg* (upper panel), *sPmP* (middle), and *sPn* (bottom).

Regional depth phases (*sPg*, *sPmP,* and *sPn*) can be used to estimate focal depth if they and their reference phases (*Pg*, *PmP,* and *Pn*) can be correctly identified. Following Langston (1987) and Bock *et al*. (1996), we developed a method to use the regional depth phases to determine focal depths. The principle is: (1) calculate synthetics with the reflectivity method (Randall, 1994) at a station with a reasonable range of depths; (2) compare the synthetics with the observed values at the same station; and (3) take as the focal depth of the earthquake the depth at which the synthetic and the observation have similar time differentials (regional depth phase to its reference phase).

We previously reported some aspects of the regional depth-phase modeling (RDPM) method (e.g., Ma *et al*., 2003; Ma and Atkinson, 2006). Here we introduce the RDPM method more systematically and describe the principles and features of the three depth phases in detail. We have proved that the assumptions of depth phase *sPmP* and its reference phase *PmP* are correct, and by conducting several tests, found in which regions the regional depth phases are developed and in which they are not, and which factors contribute to errors in the modeled focal depths. We also found that the contents of *PmP* and *sPmP* come from different interfaces beneath the source. These findings are useful for researchers who want to use the RDPM method, and especially for identifying the regional depth phases and their reference phases.

Because we use regional synthetics as a "ruler" to measure focal depth from observed waveforms, we first describe how to generate synthetics that are suitable to be used as the "ruler" and discuss some features of the regional depth phases.

2. Synthetic regional depth phases *sPg*, *sPmP*, and *sPn*

To generate synthetics we need a crustal model, earthquake location, focal mechanism, and focal depth. To generate synthetics for smaller earthquakes, the source time function is not important. We use a triangle as the source time function. Because the focal mechanism does not determine the arrival times of the seismic phases—the crustal structures determine the arrival times—the crustal model is a key factor in generating synthetic regional depth phases. Western Quebec is one of the more active seismic zones in eastern North America and the crustal structures are relatively well known. Mereu *et al*. (1986) "conducted a major long-range seismic refraction and wide-angle reflection experiment across the Grenville province of Canadian Shield," and obtained some crustal models. After studying these crustal models and modifying them slightly, we obtained one crustal model and put it in our program package as the default crustal model (Fig. 2; model 1 in Table 1). Because the focal mechanisms in western Quebec are predominantly thrust type (e.g., Adams *et al*., 1989; Bent and Perry, 1999; Ma and Eaton, 2007), we used a thrust type focal mechanism as the default (Fig. 2, bottom left).

Because regional depth phases are easier to discern on displacement records than on velocity records, we used displacement records in the RDPM. All the synthetic and observed waveforms in this chapter are the vertical component.

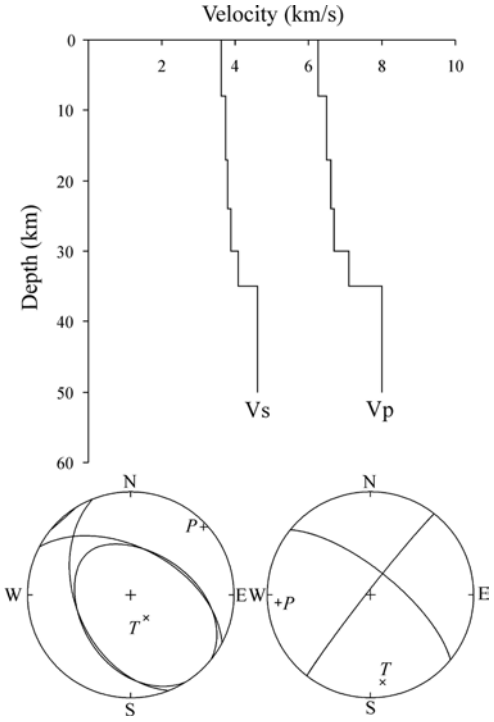

Fig. 2. The default crustal model and default focal mechanism (left; right focal mechanism is for comparison) in the RDPM method. Except if specified, all synthetic waveforms were generated with the default crustal model and default focal mechanism.

Model 1 (6 layers) h Vp Vs ρ	Model 2 (5 layers)	Model 3 (4 layers)	Model 4 (3 layers)	Model 5 (2 layers)
8 6.25 3.61 2.53	8 6.25 3.61 2.53	8 6.25 3.61 2.53	8 6.25 3.61 2.53	8 6.25 3.61 2.53
9 6.50 3.75 2.63	9 6.50 3.75 2.63	9 6.50 3.75 2.63	9 6.50 3.75 2.63	0 6.50 3.75 2.63
7 6.60 3.81 2.67	7 6.60 3.81 2.67	7 6.60 3.81 2.67	0 6.60 3.81 2.67	
6 6.70 3.87 2.71	6 6.70 3.87 2.71	0 6.70 3.87 2.71		
5 7.10 4.10 2.87	0 7.10 4.10 2.87			
0 8.00 4.62 3.23				

Table 1. The crustal models. Model 1 is the default in the RDPM program package. Crustal models 2, 3, 4, and 5 were formed by deleting the last layer successively from model 1. *h* = layer thickness (km); *Vp* = velocity of the *P*-wave (km/sec); *Vs* = velocity of the *S*-wave (km/sec); ρ = crustal density (g/cm^3).

2.1 Synthetics generated at different distances with a fixed focal depth

To observe features of the regional depth phases that are displayed when the distance changes, we generated synthetic waveforms at distances ranging from 0.3° to 4.8° and plotted them (Figs. 3, 4, and 5). Fig. 3 shows that the *sPg* phase is well developed at distances ranging from 0.7° to 0.9° (trace 070 to 090). The distance range within which *sPg* is well

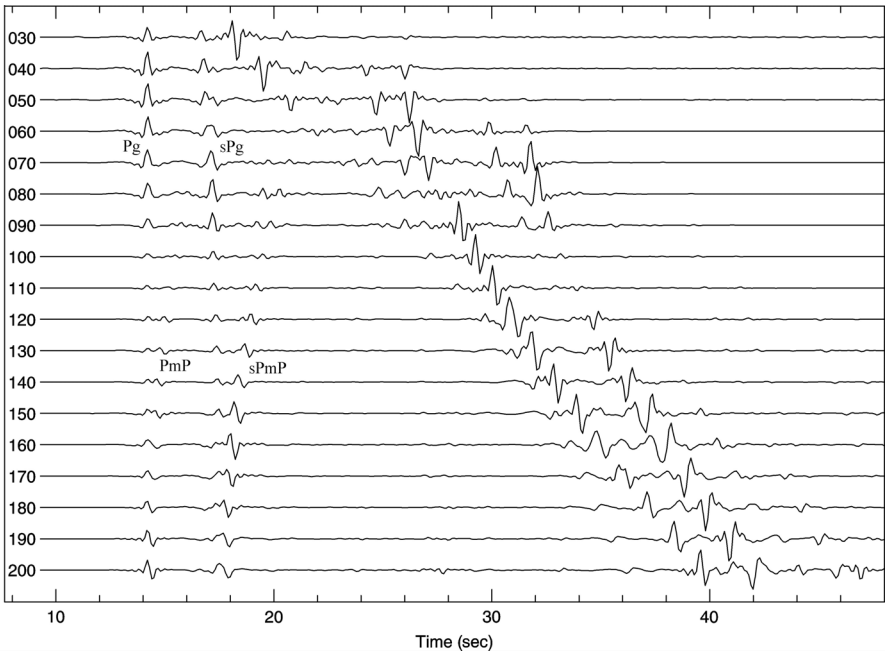

Fig. 3. Synthetic waveforms generated with depth 12 km, azimuth 236°, at distances 0.3° to 2.0° (also used to generate Figs. 4, 5, 6, 7, and 8). Trace number = distance in degrees × 100. Trace 030 was generated at distance 0.3°. Traces are aligned on the first phase. On trace 070 phases *Pg* and *sPg* and on trace 140 phases *PmP* and *sPmP* are labeled.

developed changes with focal depth: the range shifts farther as the focal depth increases. The time difference *sPg*–*Pg* changes very slightly with distance. For the distance range of about 1.0° to 1.7° (trace 100 to 170), *Pg*, *PmP*, *sPg*, and *sPmP* co-exist. Fig. 4 shows that *Pg* disappears at 1.6° (or *Pg* and *PmP* merge there; trace 160); *sPg* disappears at 1.9° (trace 190). For the distance window of about 1.8° to 2.8° (trace 180 to 280), the waveforms are quite simple. The first phase is *Pn* (generally weak); the second phase is *PmP* and the third phase is *sPmP*. Fig. 5 shows that *sPn* stands out at about 3.0° (trace 300). The time difference *sPn*–*Pn* is independent of distance. For distances larger than 2.9° (trace 290), waveforms become complex. At about 4.1° (trace 410) there is another distance window in which waveforms are relatively simple.

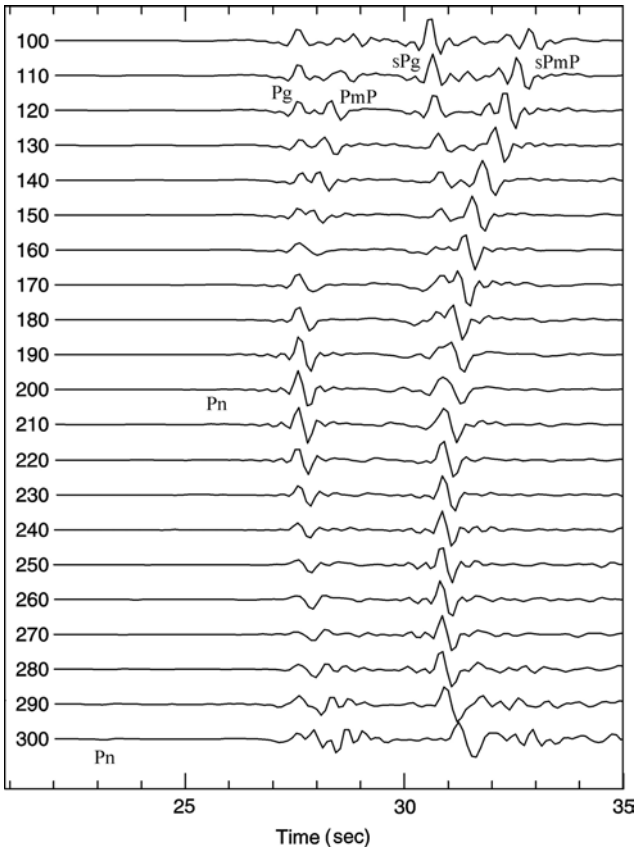

Fig. 4. Synthetic waveforms generated with depth 12 km, azimuth 236°, at distances 1.0° to 3.0°. Trace 100 was generated at distance 1.0°. Traces are aligned on *Pg* or *PmP*. The distance window in which waveforms are simple is from about 200 to 300 km (trace 180 to 280). The *Pn* phase is weak. Traces 100 to 200 correspond to the early parts of those traces with the same labels in Fig. 3, but with amplitude enlarged and timescale expanded.

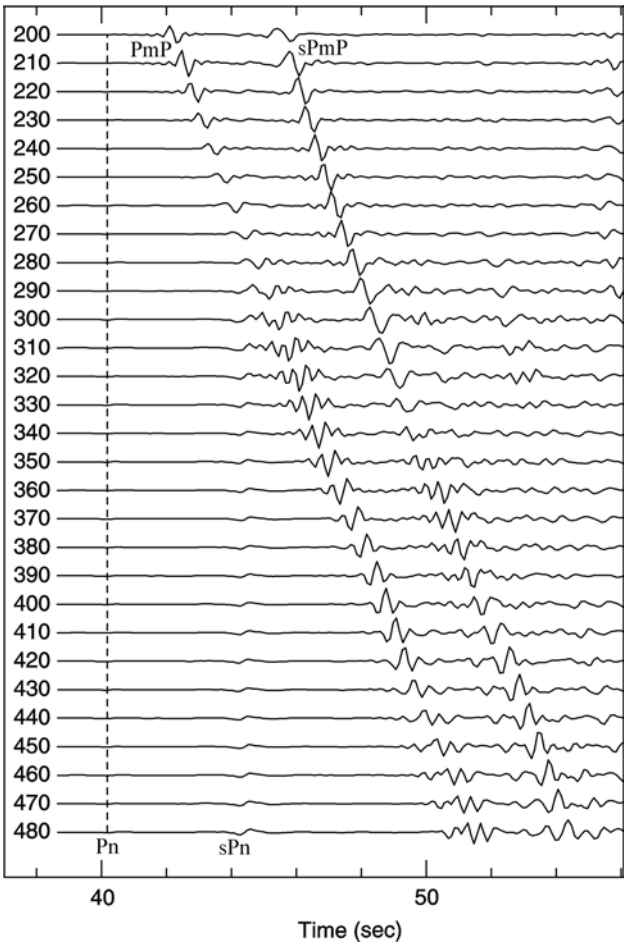

Fig. 5. Synthetic waveforms generated with depth 12 km, azimuth 236°, at distances 2.0° to 4.8°. Top trace 200 was generated at distance 2.0°. Traces are aligned on *Pn*. The *sPn* phase stands out at 3.0° (trace 300), but is buried at closer distances. After 2.8° (trace 280) waveforms become complex. Around trace 410 (4.1°) waveforms are simple again.

2.2 Synthetics generated with a range of focal depths at fixed distances

To observe how regional depth phases change with focal depth, we generated synthetic *sPg*, *sPmP*, and *sPn* with a range of depths at fixed distances 0.9°, 2.1°, and 4.1°. Fig. 6 shows that the time difference *sPg–Pg* becomes progressively larger with focal depth. The position of *sPg* shifts by about half a cycle when the depth changes by 1 km. This means that the time difference *sPg–Pg* is very sensitive to focal depth. At distance 0.9°, *sPmP* is not well developed. Fig. 7 shows that the time difference *sPmP–PmP* becomes larger as depth increases. The position of *sPmP* also shifts by about half a cycle when focal depth changes by 1 km. The *Pn* phase is also a depth phase, but it is not as sensitive as *sPmP* to focal depth. For example, on trace 210, the time difference between *Pn* and *PmP* is about half that

between *sPmP* and *PmP*. The time difference *Pn*–*PmP* changes obviously with distance (Fig. 5). These features of *Pn* can be used to identify *sPmP* in its distance window (200 to 300 km). Fig. 8 shows how the time difference *sPn*–*Pn* changes with focal depth. Because the *sPn* phase is stronger than *Pn*, it is possible that some of the observed "*Pn*" phase beyond 300 km is *sPn*.

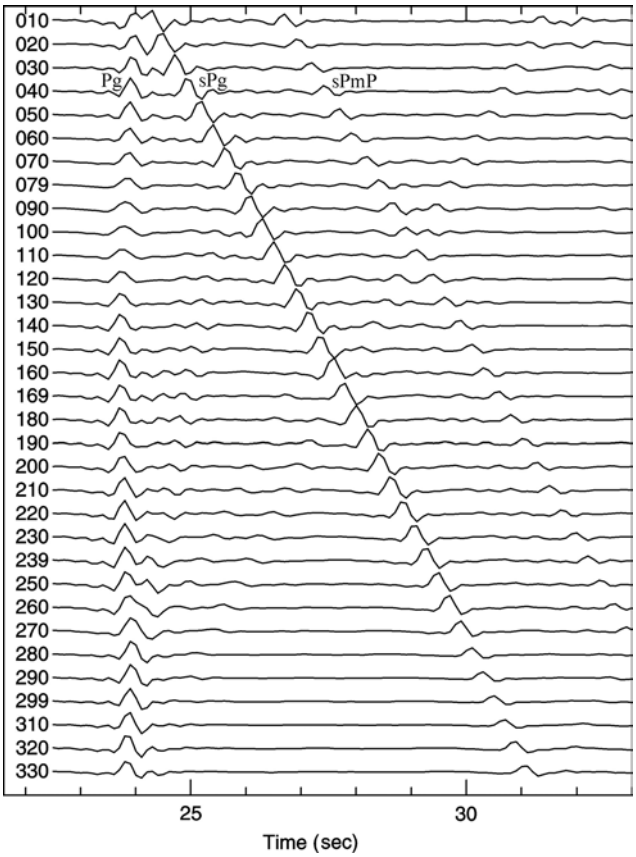

Fig. 6. Synthetic waveforms generated at distance 0.9º with depths from 1 to 33 km. Trace number = depth in km × 10. Trace 010 was generated with depth 1 km at distance 0.9°.

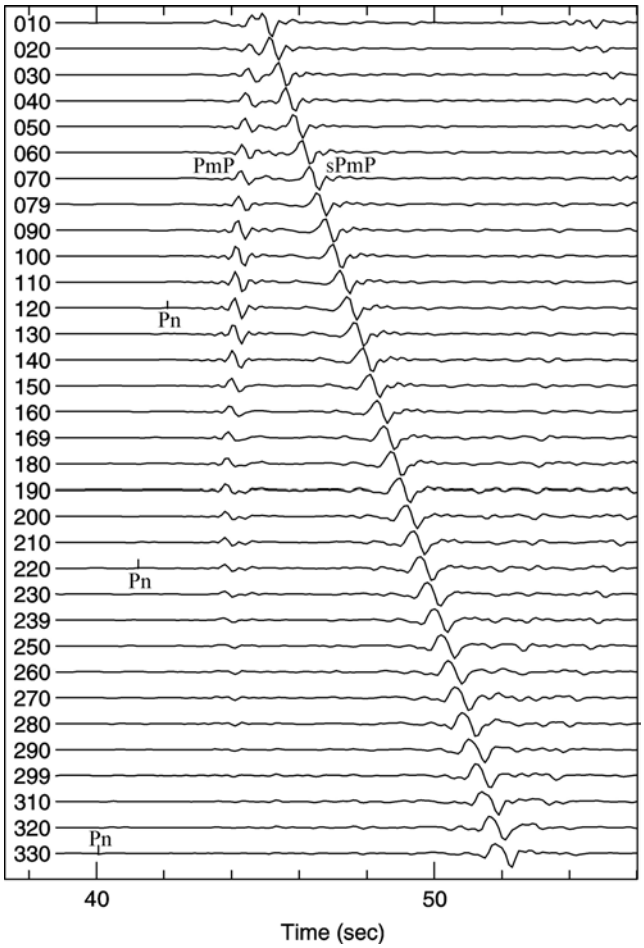

Fig. 7. Synthetic waveforms generated at distance 2.1° with depths from 1 to 33 km. Trace 010 was generated with depth 1 km at distance 2.1°. On trace 070 phases *PmP* and *sPmP* are labeled. The *Pn* phase is weak, and is labeled on traces 120, 220, and 330.

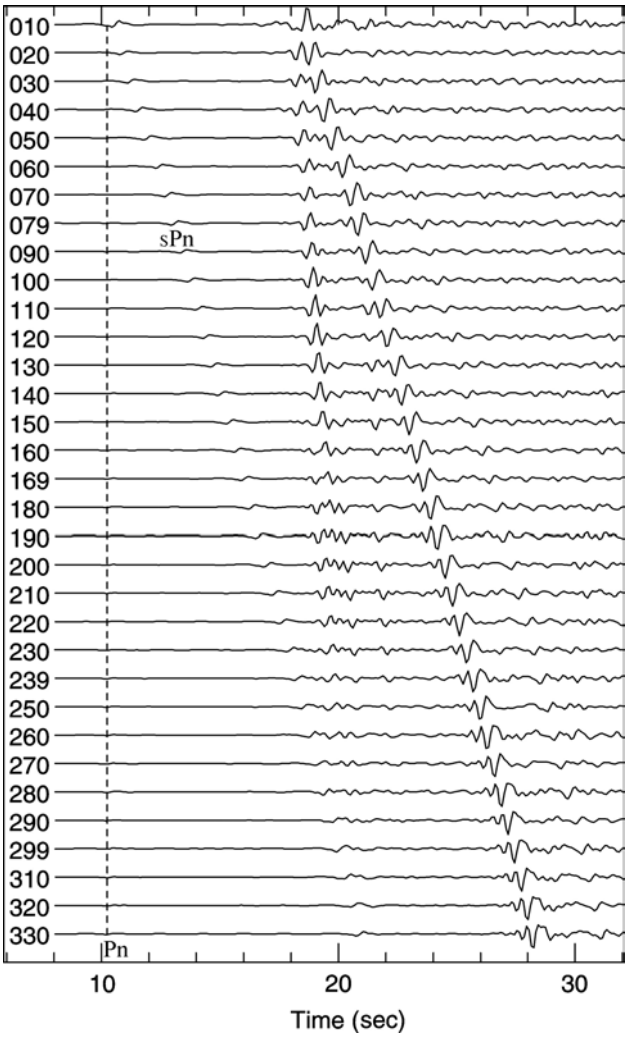

Fig. 8. Synthetic waveforms generated with depths of 1 to 33 km at distance 4.1°. Trace 010 was generated with depth 1 km at distance 4.1°. The *Pn* phase is weak; *sPn* is stronger than *Pn*. From trace 260 (26 km) *sPn* merges with other phases. Traces are aligned on the *Pn* phase.

2.3 Synthetics generated with different focal mechanisms

To generate synthetics we need a focal mechanism. Generally, no focal mechanism solutions are available for small earthquakes. To solve this problem, we used a default focal mechanism for all earthquakes to generate synthetics to measure focal depths. Because focal mechanisms do not determine the arrival times of seismic phases, we used a default focal mechanism to generate synthetic phases for their arrival times. Because we do not use waveform shapes to estimate focal depth, we do not have to use a strike–slip focal mechanism to generate synthetics for earthquakes with strike–slip focal mechanisms.

3. Demonstration for the assumed *sPmP* and *PmP* phases

In eastern North America many *P* portions of waveform records are similar to trace CRLO/EHZ in Fig. 9. On this trace, the first weak phase is *Pn*. We assumed that the second phase is *PmP* and the third phase (the largest) is *sPmP*. To demonstrate that the assumptions are correct, we prepared Fig. 9 using explosive and earthquake source models. On trace EXPL/140, no strong assumed depth phase appears at the position corresponding to that on trace CRLO/140 which was generated with the same depth and crustal model. The reason is that an explosive source does not directly generate *S*-waves. According to the definition of *sPmP*, the phase should arrive at a station progressively later as the focal depth increase because the total path length becomes longer. The third phase on traces CRLO/130, 135, 140, 145, and 150 arrives progressively later as the depth increases. This feature and the absence of the strong phase on EXPL/140 indicate that the "assumed *sPmP*" is *sPmP*.

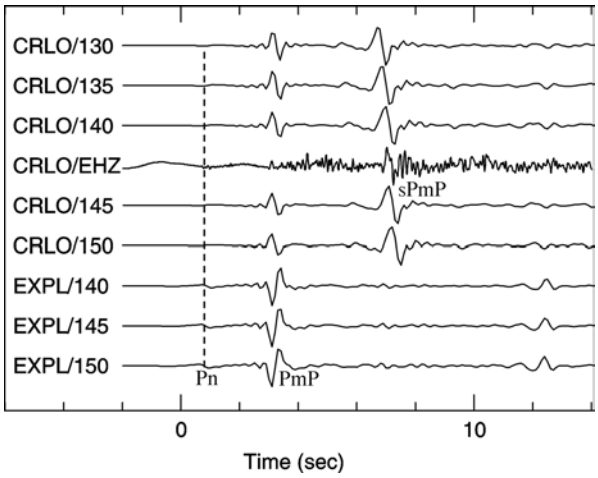

Fig. 9. Synthetic waveforms generated with an earthquake source model (Fig. 2, bottom-left) (traces CRLO/130 to 150), an explosive source model (traces EXPL/140 to 150), and the *P* portion recorded at station CRLO generated by a small earthquake (1995/09/12, m_N 3.7, west Quebec; trace CRLO/EHZ). CRLO/130 was generated with depth 13 km at distance 2.10° and azimuth 283°. EXPL/140 was generated with depths 14.0 km. Trace CRLO/EHZ is the *P* portion generated by the small earthquake. The modeled focal depth for this earthquake is 14.5 km.

To demonstrate that the phase has experienced reflection from the Moho, we prepared Fig. 10 by using different crustal models and depths. In group 2 (2/130, 2/140, 2/150), a weak *sPmP* appears. This might be because the interface at depth 8 km is above the sources. When we put the sources at the same depths in a half space, the weak *sPmP* disappears. In groups 3 (3/130, 3/140, 3/150), 4 (4/130, 4/140, 4/150), 5 (5/130, 5/140, 5/150), and 6 (6/130, 6/140, 6/150), the assumed *PmP* and *sPmP* appear and are clear. The time differences *sPmP*–*PmP* are almost the same on traces 3/130, 4/130, 5/130, and 6/130, etc. "*PmP*" and "*sPmP*" from different interfaces can pile up at similar positions. Fig. 10 demonstrates that the assumed depth phase *sPmP* experienced reflection at the Moho, because its shapes, for example, on traces 3/150, 4/150, 5/150, and 6/150, are different.

The waveform contents of the *sPmP* on trace 6/150, for example, contain contributions from all interfaces beneath the source.

From the definition of *PmP* we know that as focal depth increases, *PmP* should arrive earlier, because the total travel path becomes shorter. Generally, we use the phase recorded in the distance window of about 200 to 300 km. At these distances, the feature that *PmP* arrives earlier as focal depth increases is not easy to examine without *Pg* as the reference phase. So we traced the assumed *PmP* to close distances where *Pg* exists. Fig. 11 is the synthetic waveforms generated with an explosive source model. Trace 210 in Fig. 11 is similar to trace EXPL/140 in Fig. 9, which was generated with depth 14 km at distance 2.10°. Let us trace the assumed *PmP* in Fig. 11 from trace 080 to trace 150 where both *Pg* and the assumed *PmP* exist. At such a close distance, the first phase is *Pg*. We then generated synthetics at fixed distance 0.8° with depths of 1.0 to 35.0 km (Moho depth). Fig. 12 shows that the two phases become closer as depth increases, and they merge at the Moho. This test shows that the assumed *PmP* is *PmP*. Based on these tests, the assumed phases *PmP* and *sPmP* on trace CRLO/EHZ are *PmP* and *sPmP*, because these two phases have the same features as those on traces CRLO/130 to CRLO/150.

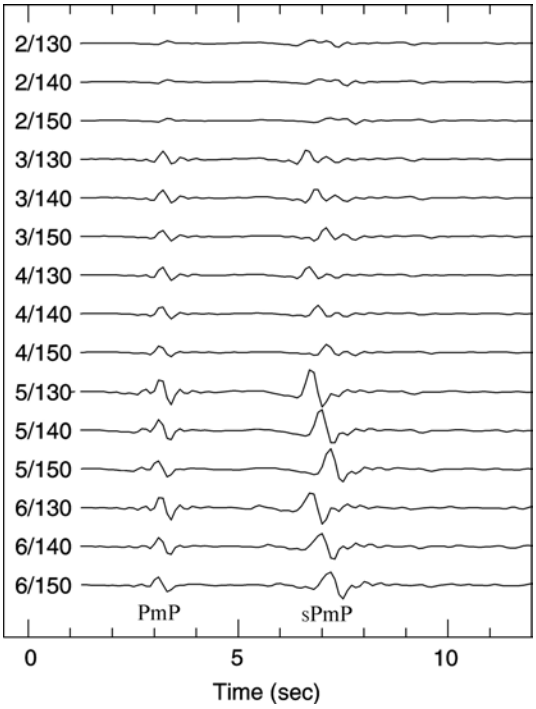

Fig. 10. Synthetic waveforms generated with the five crustal models listed in Table 1 at distance 2.10° and with depths 13, 14, and 15 km. Trace Group 2 (2/130, 2/140, 2/150) was generated with a two-layer crustal model (Model 5 in Table 1); Group 3 with a three-layer crustal model (Model 4 in Table 1); Group 4 with a four-layer crustal model (Model 3 in Table 1); Group 5 with a five-layer crustal model (Model 2 in Table 1); Group 6 with a six-layer crustal model (Model 1 in Table 1).

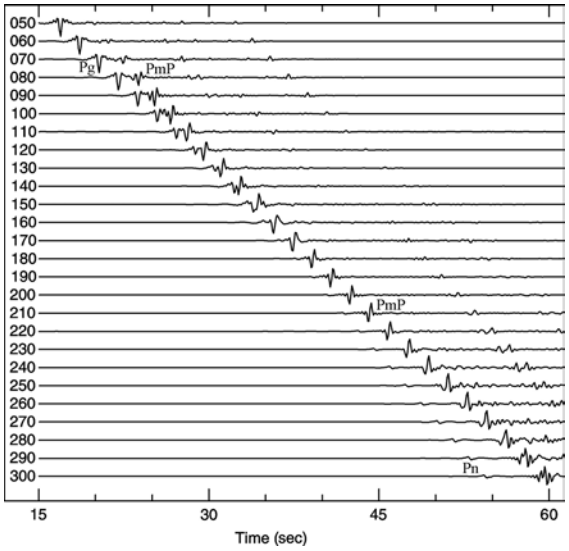

Fig. 11. Synthetic waveforms generated with depth 13 km, an explosive source model, and crustal model 1 in Table 1, at distances of 0.5° to 3.0°. Trace 210 was generated at 2.10°. The *Pg* phase disappears at about 1.5° (trace 150). The *PmP* phase is clear from 1.7° to 2.8° (traces 170 to 280).

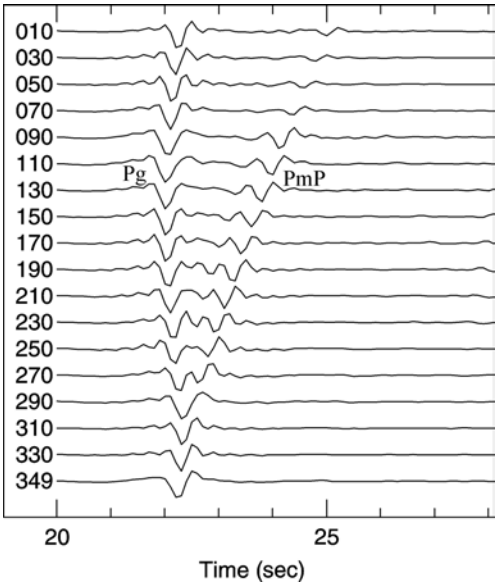

Fig. 12. Synthetic waveforms generated at distance 0.8° with depths of 1.0 to 34.9 km, an explosive source model, and crustal model 1 in Table 1. Trace 130 in this figure is the same as trace 080 in Fig. 11. Because the total path length becomes shorter with focal depth, the *PmP* phase arrives progressively earlier with depth.

4. Comparison of RDPM focal depths with those from other methods

In eastern Canada and the New York State region, some moderate and strong earthquakes have reliable focal depth solutions. For the same earthquakes we compared focal depth solutions obtained by RDPM with those obtained by other methods. We found that the consistency is good.

4.1 *sPn* modeling for the M_W 5.0 2002/04/20 Au Sable Forks, New York earthquake

We analyzed the waveform records for this earthquake and found many *sPn* records. We modeled the *sPn* and *Pn* phases recorded at a POLARIS station, Canada (Fig. 13). From *sPn* and *Pn* paths in a one-layered crustal model of Poisson medium, the following equation calculates focal depth using the time difference *sPn*–*Pn*:

$$t(h;sPn-Pn)=\frac{h}{V_{p1}}\left[\sqrt{3-k^2}+\sqrt{1-k^2}\right]; \tag{1}$$

where $k=V_{p1}/V_{p2}$; V_{p1} and V_{p2} are *P*-wave velocities in and beneath the crust, respectively; h is the focal depth; and t is the differential time. The differential time is independent of station distance and crustal thickness. Even if we have only one pair of reliable *sPn* and *Pn* observations, we can obtain a focal depth solution with a small error without considering the earthquake location error. The time difference *sPn*–*Pn* on trace ACTO/HHZ is 4.06 sec. When we take V_{p1} = 6.25 km/sec and V_{p2} = 8.0 km/sec, the focal depth from equation (1) is 11.7 km; this depth is close to the focal depth (about 11.5 km) determined by RDPM.

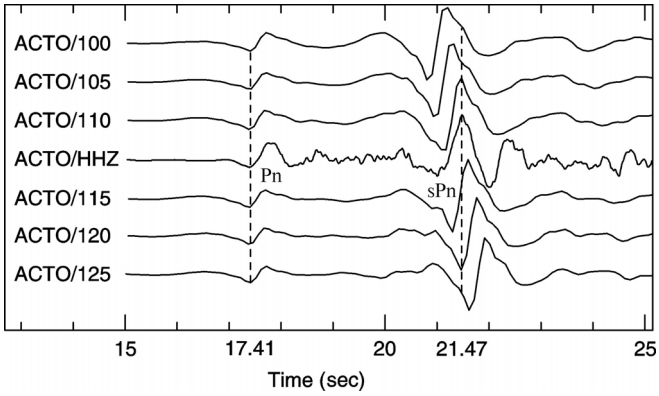

Fig. 13. Phase *sPn* modeling for 2002/04/20 Au Sable Forks, New York, M_W 5.0 earthquake. Trace ACTO/100 was generated with depth 10 km at station ACTO (517 km). Trace ACTO/HHZ is the earthquake observation; it matches a trace somewhere between ACTO/110 and ACTO/115. We can take 11 km or 11.5 km as the modeled focal depth. The time difference *sPn*–*Pn* on trace ACTO/HHZ is 4.06 sec. Using this number in equation (1) gives a focal depth of 11.7 km.

To compare the RDPM depth, we analyzed the teleseismic depth phase *sP* and its reference phase *P* at YKA (Yellowknife Array, Canada). Fig. 14 shows some of the records. The time difference *sP*–*P* is 4.85 sec. The following equation calculates focal depth from differential time:

$$t(h,\alpha;sP-P)=\frac{h}{V_p\sqrt{1-\frac{1}{3}\sin^2\alpha}}\left(\sqrt{3}+1-\frac{4}{3}\sin^2\alpha\right); \quad (2)$$

where V_P is the *P*-wave velocity in a one-layered crustal model of Poisson medium, a is the *P*-wave take-off angle, t is the differential time, and h is the focal depth. If we take V_P = 6.25 km/sec and a = 29.68° the focal depth from equation (2) is 12 km.

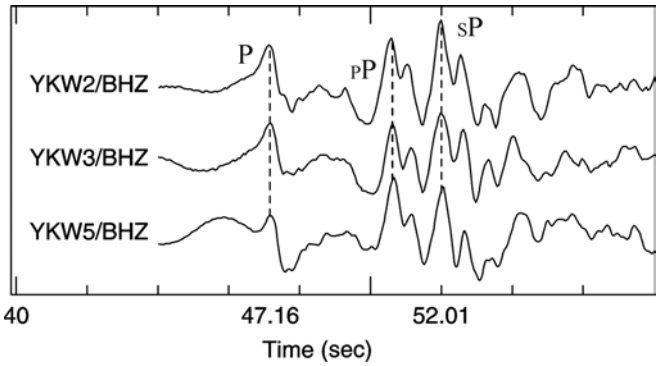

Fig. 14. Teleseismic depth phases records of 2002/04/20 Au Sable Forks, New York, M_W 5.0 earthquake at YKA (Yellowknife Array, Canada). Based on the time difference *sP*–*P* (4.85 sec), the focal depth from equation (2) is about 12 km.

4.2 s*Pg* modeling for the m_N 4.3 1993/11/16 Montreal south earthquake and its aftershocks

Many *sPg* (and *sPmP*) records are available in eastern Canada and New York region. As an example we selected the records from station MNT (37 km from a main shock and its

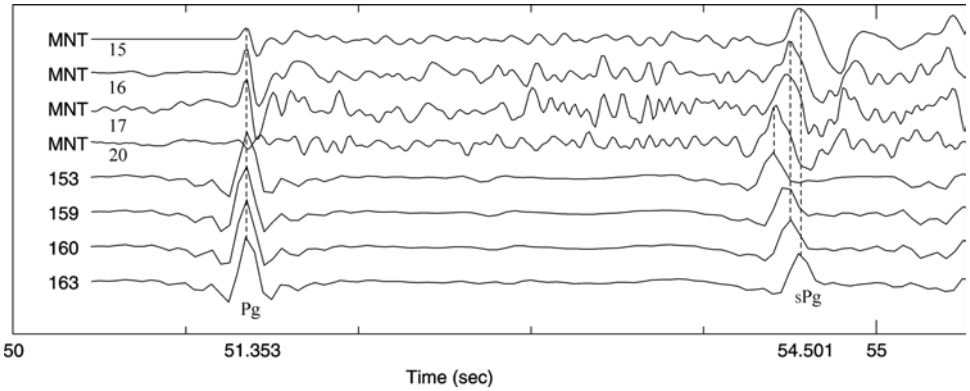

Fig. 15. *sPg* and *Pg* modeling for earthquakes No. 15, 16, 17, and 20 in Table 2 of Ma, 2010. Traces labeled 15, 16, 17, and 20 are *P* portions recorded at station MNT (37 km). Traces 153, 159, 160, and 163 are synthetics generated with depths 15.3, 15.9, 16.0, and 16.3 km at station MNT. The subtle differential times *sPg*–*Pg* show that these earthquakes occurred on a fault that ruptured about 1 km at depth about 15 km.

aftershocks; No. 15, 16, 17, and 20 in Table 2 of Ma, 2010). Fig. 15 shows that the main shock is the deepest and the last aftershock is the shallowest, and the depth difference between, for example, No. 15 and 16, is about 0.3 km.

4.3 *sPmP* modeling for the M_L 5.1 1983/10/07 New York region earthquake and its aftershock (No. 5 in Table 2 of Ma 2010)

We selected the records from station SBQ (244 km) as an example. In Fig. 16, trace SBQ/SHZ 10:18:12.0 is the record of the main shock at station SBQ, and trace SBQ/SHZ 10:39:06.0 is the record of its aftershock. From the time differences *sPmP*–*PmP* on the synthetics SBQ/079 and SBQ/085, we found that the aftershock is shallower than the main shock by about 0.5 km. The modeled focal depth for the main shock is 8.5 km. The focal depth obtained by the Geological Survey of Canada is 10.0 km. From the first record we see the *Pn* phase clearly, but from the second record we cannot. This means that the *Pn* phase disappeared or was too weak to be measured.

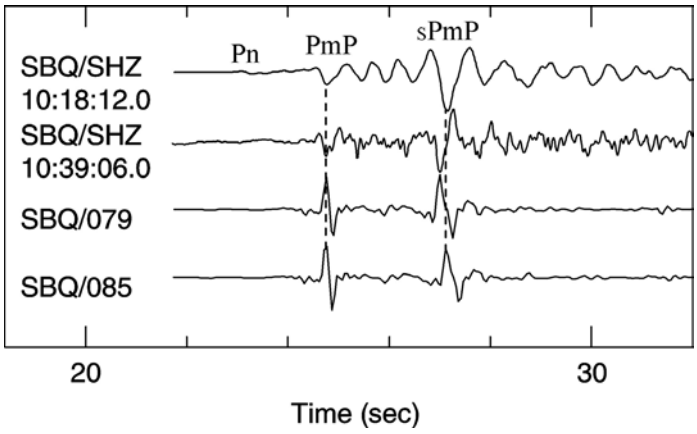

Fig. 16. *sPmP* and *PmP* modeling for earthquake No. 5 in Table 2 of Ma, 2010 and one of its aftershocks (1983/10/07 10:39:39.0, M_L3.5). The top trace is the record of the earthquake at station SBQ; the second trace is the record of the aftershock. Traces SBQ/079 and SBQ/085 are synthetic waveforms generated with depths 7.98 and 8.5 km at station SBQ. The subtle differential times *sPmP*–*PmP* show that the two earthquakes occurred at different depths. On the second trace the *Pn* phase is not measurable.

4.4 *sPmP* modeling for two aftershocks of the M_W 6.5 2003/12/22 California earthquake

Many regional records are available for the main shock and its aftershocks. We retrieved the records of some aftershocks at stations within 5° from IRIS for analysis. We found that two aftershocks have clear *sPmP* phase records at stations VCS (2.76°), CHF (2.89°), PAS (2.87°), and MWC (2.92°). We modeled the *sPmP* and *PmP* at station PAS, and obtained focal depths 6.5 km for the 05:30 event and 6 km for the 18:17 event (Fig. 17). The preliminary focal depths obtained by the local network for the two aftershocks are 5.9 km and 6.9 km, respectively.

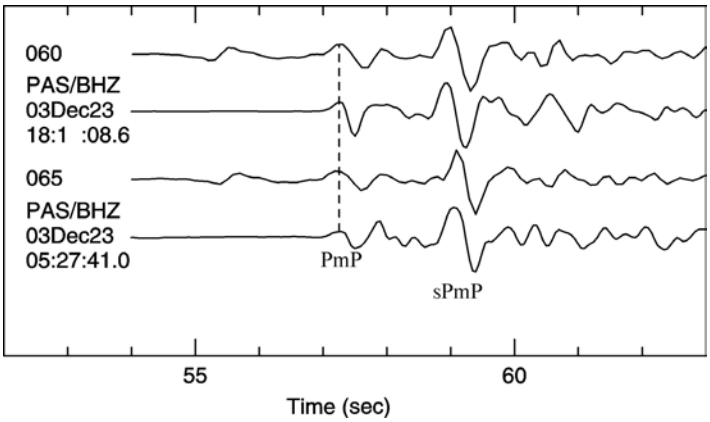

Fig. 17. *sPmP* and *PmP* modeling for two aftershocks of the 2003/12/22 Central California M_W 6.5 earthquake. Trace PAS/BHZ/03Dec23 18:15:08.6 is the record of the aftershock 2003/12/23/ 18:17:11.0 *M* 4.9 at station PAS. Trace PAS/BHZ/03Dec23 05:27:41.0 is the record of the aftershock 2003/12/23/ 05:30:19.0 *M* 4.5. Traces 060 and 065 are the synthetic waveforms generated with depths 6 and 6.5 km at the same station (320 km). The focal depth solution for the 18:17 event is 6 km and for the 05:30 event is 6.5 km.

5. Possible errors in the modeled focal depth

We used the differences in arrival times between synthetic regional depth phases and their reference phases to measure focal depth from the observations. The *P*- and *S*-wave velocities in the crustal model determine the arrival times of these phases. When we generate synthetics we also need the focal mechanism and the earthquake location, but the errors generated by these two factors are negligible.

5.1 The error in the modeled focal depth caused by the crustal model

Travel times of regional depth phases and their reference phases are determined by the crustal structures through which the phases propagate. As such, most of the error in modeled focal depths comes from the crustal velocity model used.

(A) The error caused by the velocity model

To evaluate errors arising from velocity uncertainty in the crustal model, we generated synthetic seismograms (at an epicentral distance of 2.16°) using our default crustal model given in Table 1 (model 1), with focal depths from 2 to 23 km. We then reduced the *P*- and *S*-wave velocities of the crustal model by 10% and generated another set of synthetics with the same distance and depths. Fig. 18 (Ma and Eaton, 2011) shows the differential times between *sPmP* and *PmP* phases for these two models. The time delay obtained by subtracting these differential times is approximately linear with focal depth. Focal depths, estimated using the RDPM method by treating one set of synthetic traces as observed seismograms, differ by 9.5 – 12% (Fig. 18, bottom). The differences are on the order of 11%, slightly greater than the 10% change in velocity. These numerical tests indicate that the level of uncertainty in the velocity model propagates, at approximately the same order of magnitude, into focal-depth uncertainty.

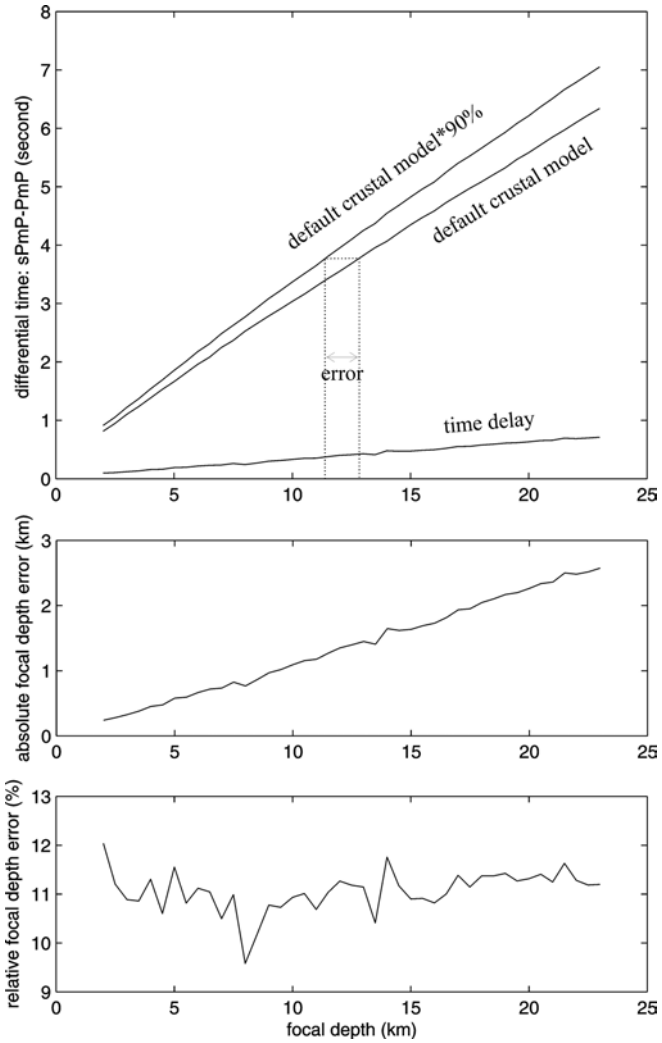

Fig. 18. Errors in the modeled focal depth caused by errors in the crustal model. The upper panel shows the differential times between *sPmP* and *PmP* generated by the default crustal model and by a low-velocity model (90% of the default crustal model). The intersection points between the vertical faint lines and the depth axis are focal depth solutions obtained by the two tiled lines from the same differential time *sPmP-PmP* (the height of the faint line bar). The difference between the two solutions is the absolute error. The middle panel shows how the absolute errors change with focal depth. The bottom panel shows the relative errors.

(B) The error caused by the Vp/Vs ratio

We assumed that the crustal media are Poisson type in which Vp/Vs is 1.732. To examine the possible error in our modeled focal depth caused by the Poisson assumption, we made

the following tests: (1) We made one new ratio by adding 5% to 1.732 and used the ratio and the Vp values in our default crustal model to create one crustal model *M*1. (2) We subtracted 5% from 1.732 to form a second new ratio and used this ratio to create crustal model *M*2. We compared the synthetics generated using these two crustal models and the default model and found that the time differences *sPmP–PmP* on traces generated with *M*1 and depth 11.2 km, generated with *M*2 and depth 12.9 km, and generated with the default crustal model and depth 12 km are approximately equal. This shows that when the crustal medium differs from the Poisson medium by 5%, the relative error in modeled focal depth is less than 8%.

(C) The error caused by strong interfaces in the crust

Our default crustal model assumes five layers. The thickness of the fourth layer is 6 km (Model 1 in Table 1). We divided the layer into two parts of equal thickness, keeping the original velocities in the upper layer, but changing the velocities in the lower layer to those of the third layer. We generated synthetics with this new crustal model and the default focal mechanism at distance 2.13° (Fig. 19). The time difference *sPmP–PmP* does not change noticeably (on traces 120 and STD), but the shape of "*sPmP*" broadened. This change shows that the *sPmP* phase is not a simple phase; it has the "*sPmP*" from the interface where Vp = 6.6 and 7.1 km/sec; Vs = 3.81 and 4.1 km/sec in the new crustal model. This change demonstrates that if there are strong interfaces above the Moho, the *sPmP* phase can be complex, and can cause time-reading errors.

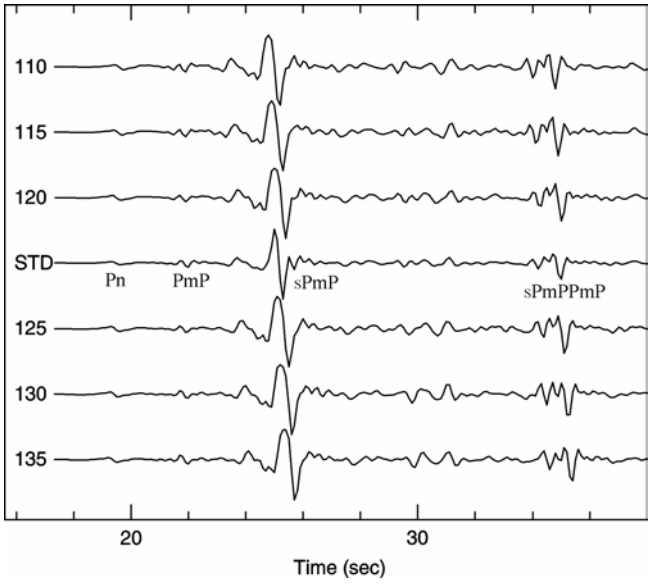

Fig. 19. Synthetic waveforms generated with the default crustal model and a new crustal model that contains a weak lower velocity layer. Trace 110, 115, 120, 125, 130, and 135 were generated with the new model and depth 11, 11.5, 12, 12.5, 13, and 13.5 km. Trace STD was generated with the default crustal model and depth 12 km.

Model 1 h Vp Vs ρ	Model 2	Model 3	Model 4	Model 5	Model 6
1 1.25 0.72 0.51	1 2.25 1.30 0.91	1 3.25 1.88 1.31	1 4.25 2.45 1.72	1 5.25 3.03 2.12	1 6.25 3.61 2.53
7 6.25 3.61 2.53	7 6.25 3.61 2.53	7 6.25 3.61 2.53	7 6.25 3.61 2.53	7 6.25 3.61 2.53	7 6.25 3.61 2.53
9 6.50 3.75 2.63	9 6.50 3.75 2.63	9 6.50 3.75 2.63	9 6.50 3.75 2.63	9 6.50 3.75 2.63	9 6.50 3.75 2.63
7 6.60 3.81 2.67	7 6.60 3.81 2.67	7 6.60 3.81 2.67	7 6.60 3.81 2.67	7 6.60 3.81 2.67	7 6.60 3.81 2.67
6 6.70 3.87 2.71	6 6.70 3.87 2.71	6 6.70 3.87 2.71	6 6.70 3.87 2.71	6 6.70 3.87 2.71	6 6.70 3.87 2.71
5 7.10 4.10 2.87	5 7.10 4.10 2.87	5 7.10 4.10 2.87	5 7.10 4.10 2.87	5 7.10 4.10 2.87	5 7.10 4.10 2.87
0 8.00 4.62 3.23	0 8.00 4.62 3.23	0 8.00 4.62 3.23	0 8.00 4.62 3.23	0 8.00 4.62 3.23	0 8.00 4.62 3.23

Table 2. New crustal models generated by dividing the first layer in the default model (Table 1) into two parts, making the first part 1-km thick, and changing the *P*- and *S*-wave velocities in that layer in steps. *h* = layer thickness (km); *Vp* = velocity of the *P*-wave (km/sec); *Vs* = velocity of the *S*-wave (km/sec); ρ = crustal density (g/cm^3).

5.2 The error caused by an error in earthquake location

To estimate the error in the modeled focal depth caused by the error in earthquake location we can observe Fig. 4 or 5 (or Uski *et al*., 2003; their Fig. 2). In the distance window of 1.8^o to 3.0^o, when the distance changes, for example, 0.1^o (~11 km) at distance 2.2^o, the time difference *sPmP*–*PmP* is almost constant. This means that when the earthquake location has an 11-km error in the above distance window, the error in the modeled focal depth caused by the error in earthquake location is negligible.

5.3 The error caused by the focal mechanism

Focal mechanism determines the radiation pattern of seismic waves but it does not determine arrival times of seismic phases (e.g., Ma and Atkinson, 2006; their Fig. 11). However, the focal mechanism partially determines the shapes and amplitudes of waveforms and thus may cause an error in time readings. If the observed *PmP* and *sPmP* are clear, but the synthetic *PmP* or *sPmP* are not, we can change the station azimuth, generate new synthetics, and then make comparisons again. So, the arrival time reading error caused by the focal mechanism is negligible. To reduce the reading error, we use the arrival times of peaks of *sPmP* and *PmP*.

6. Possible factors that determine the development of the regional depth phases

Many factors determine the development of regional depth phases. The key factors are the crustal structures at the free surface and at the Moho. We tested the effect of crustal structure at the free surface on the development of the regional depth phases. We divided the first layer of the default crustal model into two parts, making the first layer 1-km thick. We changed the velocities in the new first layer gradually to obtain new crustal models (Table 2). For each new crustal model, we generated synthetics with depth 12 km at distance 2.20°. Fig. 20 shows that on traces 020, 030, 040, 050, 125, and 225, the depth phase *sPmP* is not discernible. On traces 010, 325, and 425, *sPmP* is not prominent. On traces 001, 005, 525, and 625, *sPmP* is clear. Based on this test, we may say that if there is a sedimentary layer in the source region (reflecting sites) and the layer is sufficiently thick, the *sPmP* phase is not developed.

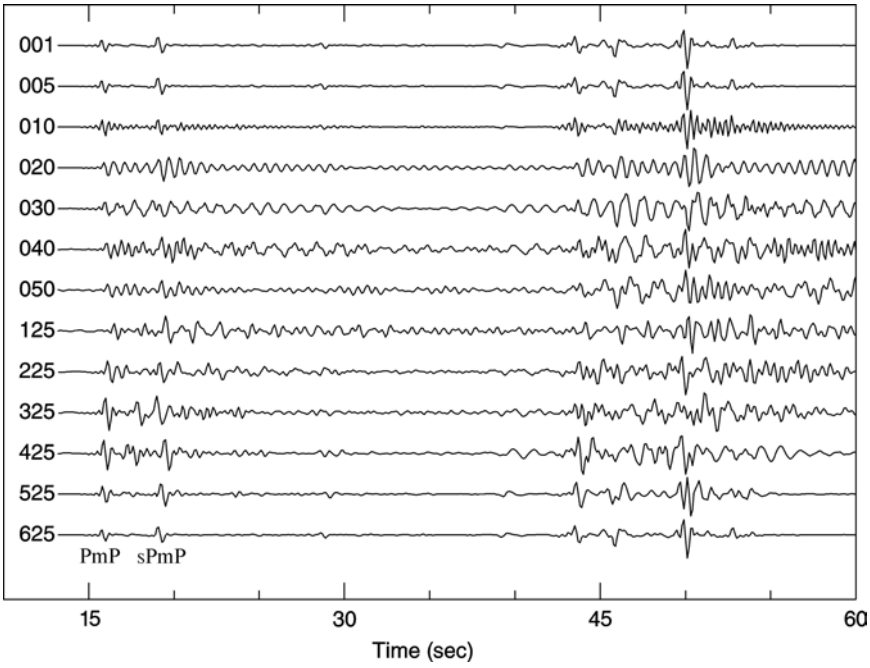

Fig. 20. Synthetic waveforms generated with the new crustal models listed in Table 2 at distance 2.20° and depth 12 km. Trace 125 was generated with Model 1 in Table 2; trace 225 with Model 2; trace 325 Model 3; trace 425 Model 4; trace 525 Model 5; trace 625 Model 6. Trace 001, 005, 010, 020, 030, 040 and 050 were generated with Model 1, but the thickness of the first layer was changed in steps to 0.01, 0.05, 0.1, 0.2, 0.3 0.4, and 0.5 km, successively.

7. Outline of the procedure to identify the regional depth phases

There are distance windows in which regional depth phases are developed. Phase *sPg* is developed well within 100 km, *sPmP* is developed well within about 200 to 300 km, and *sPn* is developed at more than 300 km. Figs. 3, 4, and 5 show these distance windows. Because time differences *sPg–Pg*, *sPmP–PmP,* and *sPn–Pn* are not sensitive to station distance, we can align all records generated by an earthquake by station distance to identify these regional depth phases.

The procedure has the following steps:

1. Retrieve the catalogue from the official website of GSC (Geological Survey of Canada);
2. Select an earthquake to determine its focal depth using RDPM;
3. Retrieve the pick file for the earthquake;
4. Retrieve all the available waveform records from the same website;
5. Based on the station distances in the pick file, arrange/display the waveform records;
6. In the above distance windows, align the records first and then search the regional depth phase and its reference phase pairs.

If two pairs (one pair = regional depth phase and its reference phase) on two records at two stations have similar differential times, the pairs may be treated as candidates for modeling.
We can model one pair or two pairs using RDPM to obtain the focal depth. The modeling procedure is shown in Fig. 9. If only one record is available at a distance window, the period feature (*sPg*, *sPmP*, and *sPn* have longer periods than their respective reference phases) may be used for the identification. The feature that *Pn*, *PmP*, and *sPmP* have relative positions on the record (see Fig. 7) can also be used to identify *sPmP* and *PmP*. Dineva *et al.* (2007; their Fig. 9) provided an excellent example for regional depth phase identification.
If more than one station has regional depth phase records for the same earthquake, the focal depth solutions obtained at different stations should be similar (see Ma and Atkinson, 2006; their Table 1).

8. Summary and discussion

There are many small earthquakes in eastern North America. These earthquakes do not have measurable teleseismic depth phases, and generally do not have close (<40 km) waveform records. No focal depths can be reliably estimated with either teleseismic depth phases or close seismic signals for most of these earthquakes, but the depths are crucial information for many topics, both theoretical and applied.
On regional waveform records, one or more phases are well developed between the first arrivals (*Pg* or *Pn*) and the *S*-wave train, and one or two of them are regional depth phases. Within about 100 km, the *sPg* phase is well developed on some records of earthquakes as small as m_N 1.5. In the distance window from about 200 to 300 km, the *sPmP* phase is well developed on some records of earthquakes as small as m_N 2.0. Beyond 300 km, the *sPn* phase is developed on some records of moderate and sub-moderate earthquakes. All these regional depth phases can be used to estimate focal depth.
When we generate synthetic depth phases, we use a default crustal model and default focal mechanism, and even a default station azimuth and default instrument response. In this way, we can conveniently generate synthetics for any small earthquake, and use the synthetic depth phases to estimate focal depth for that earthquake, if the arrival time difference between one observed depth phase and its reference phase is available.
We compared our modeled focal depths with those that were reliably obtained by other methods and found that the consistency in the comparisons is good.
The errors in our modeled focal depths are caused mainly by the crustal model used. The relative errors due to crustal model are estimated as within 15% when the error in the crustal velocity model is 10%, or when the thicknesses of layers in the crustal model have some errors, or the crustal medium differs from the assumed Poisson medium.
We have analyzed the regional depth phases for many earthquakes (Ma and Atkinson, 2006; Kim *et al*., 2006; Dineva *et al*., 2007; Ma and Eaton, 2007; Atkinson *et al*., 2008). For this chapter we selected some special cases to show that our modeling method is simple, reliable, and suitable for all regions where regional depth phases are developed.

9. Acknowledgments

This chapter was adapted with permission from the paper "Focal Depth Determination for Moderate and Small Earthquakes by Modeling Regional Depth Phases *sPg*, *sPmP*, and *sPn*" published by *Bull. Seism. Soc. Am*. It covers the author's long-time research results. Most of

the research is from time spent as a Visiting Fellow at the Geological Survey of Canada, Ottawa, where colleagues Dr John Adams, David McCormack, and Veronika Peci provided key references and made useful suggestions. Part of the research is from post-doctoral work at Carleton University, Ottawa. Two anonymous reviewers provided constructive recommendations that improved that paper dramatically. BSSA Associate Editor Lorraine W. Wolf proved helpful suggestions for publication of this superficially simple but important paper. The efforts from the staff at the InTech - Open Access Publisher make the publication of this chapter possible. The author is grateful for all assistance listed above.

10. References

Adams, J., A. Vonk, D. Pittman, and H. Vatcher (1989). *New focal mechanisms for south eastern Canada earthquakes*, Vol. II, Geol. Surv. Canada, Open File 1995.

Aki, K., and P. G. Richards (1980). *Quantitative seismology, theory and methods*, Vol. II., W.H. Freeman and Co., San Francisco.

Atkinson, G., S. Kaka, D. Eaton, A. Bent, V. Peci, and S. Halchuck (2008). A very close look at a moderate earthquake near Sudbury, Ontario, *Seism. Res. Lett.*, 79, 119–131.

Bent, A. L., and C. Perry (1999). *Focal mechanisms for eastern Canada earthquakes: 1 January 1996–30 June 1998*, Geol. Surv. Canada, Open File 3698.

Bent, A. L., and C. Perry (2002). Depths of eastern Canadian earthquakes from regional data, *Seism. Res. Lett.* 73, 273–284. Bock, G. (1993). Depth phases from local earthquakes, *BMR J. Austr. Geol. Geophy.*, 13, 275–279.

Bock, G., G. Grunthal, and K. Wylegalla (1996). The 1985/86 Western Bohemia earthquakes: Modeling source parameters with synthetic seismograms, *Tectonophysics* 261, 139–146.

Dineva, S., D. Eaton, S. Ma, and R. Mereu (2007). The October 2005 Georgian Bay (Canada) earthquake sequence: Mafic dykes and their role in the mechanical heterogeneity of Precambrian crust, *Bull. Seism. Soc. Am.* 97, 457–473.

Ebel, J. (1995). Analysis of digital waveforms in the northeastern U.S. for source depth and strong ground motion information, report to USGS, Weston Observatory, Dep. Geol. and Geophys., Boston College.

Goldstein, P., and D. Dodge (1999). Fast and accurate depth and source mechanism estimation using *P*-waveform modeling: A tool for special event analysis, event screening, and regional calibration, *Geophys. Res. Lett.* 26, 2569–2572.

Helmberger, D., and G. Engen (1980). Modeling the long-period body waves from shallow earthquakes at regional ranges, *Bull. Seism. Soc. Am.* 70, 1699–1714.

Kim, Won-Young, S. Dineva, S. Ma, and D. Eaton (2006). The 4 August 2004, Lake Ontario, earthquake, *Seism. Res. Lett.* 77, 65–73. King, R. (1979). Observations of *sPn* from Swabian Alb earthquakes at the GRF array, *J. Geophys.* 45, 337–340.

Langston, C. (1987). Depth of faulting during the 1968 Meckering, Australia, earthquake sequence determined from waveform analysis of local seismograms, *J. Geophys. Res.* 92, 11561–11574.

Langston, C. (1996). The S*sPmP* phase in regional wave propagation, *Bull. Seism. Soc. Am.*, 86, 133–143.

Langston, C., A. Nyblade, and T. Owens (2003). Regional wave propagation in Tanzania, East Africa, *J. Geophys. Res.* 107, ESE 1-1 to 1-18.

Ma, S., and G. Atkinson (2006). Focal depth distribution for earthquakes with $m_N \geq 2.8$ in western Quebec, southern Ontario and northern New York, *Bull. Seism. Soc. Am.* 96, 609–623.

Ma, S., and D. Eaton (2007). The western Quebec seismic zone (Canada): Clustered, mid-crustal seismicity on a Mesozoic hotspot track, *J. Geophys. Res*. 112, B06305, doi:10.1029/2006JB004827.

Ma, S., V. Peci, J. Adams, and D. McCormack (2003). Routine estimate of focal depths for moderate and small earthquakes by modeling regional depth phase *sPmP* in eastern Canada, 2003 EGS-AGU-EUG Joint Assembly, Nice, France, April 2003; contribution EAE03-A-06176.

Ma, S. (2010). Focal Depth Determination for Moderate and Small Earthquakes by Modeling Regional Depth Phases *sPg*, *sPmP*, and *sPn, Bull. Seism. Soc. Am*. 100, 1073-1088.

Ma, S., and D. Eaton (2011). Combining double-difference relocation with regional depth-phase modelling to improve hypocentre accuracy, *Geophysical Journal International*; DOI: 10.1111/j.1365-246X.2011.04972.

Mereu, R., D. Wang, O. Kuhn, D. Forsyth, A. Green, P. Morel, G. Buchbinder, D. Crossley, E. Schwarz, R. DuBerger, C. Brooks, and R. Clowes (1986). The 1982 COCRUST seismic experiment across the Ottawa–Bonnechere Graben and Grenville Front in Ontario and Quebec, *Geophy. J. R. Astr. Soc*. 84, 491–514.

Mulder, T., and M. Lamontagne (1990). Analysis of CLTN traces from events in the Saguenay region, internal report, Geol. Surv. Canada (Chalevoix Local Telemetered Network).

North, R., R. Wetmiller, J. Adams, F. Anglin, H. Hasegawa, M. Lamontagne, Du Berger, L. Seeber, and J. Armbruster (1989). Preliminary results from the November 25, 1988 Saguenay (Quebec) earthquake, *Seism. Res. Lett*. 60, 89–93.

Randall, G. (1994). Efficient calculation of complete differential seismograms for laterally homogeneous earth models, *Geophys. J. Int*. 118, 245–254.

Saikia, C. (2000). A method for path calibration using regional and teleseismic broadband seismograms: Application to the 21 May 1997 Jabalpur, India earthquake (M_W 5.8), *Curr. Sci*. 79, 1301–1315.

Saikia, C., B. Woods, and H. Thio (2001). Calibration of the regional crustal waveguide and the retrieval of source parameters using waveform modeling, *Pure Appl. Geophys*. 158, 1301–1338.

Savage, B., J. Chen, and D. Helmberger (2003). Velocity variation in the upper-most mantle beneath the southern Sierra Nevada and Walker Lane, *J. Geophys. Res*. 108, B7.

Somerville, P., J. McLaren, C. Saikia, and D. Helmberger (1990). The 25 November 1988 Saguenay, Quebec, earthquake: Source parameters and the attenuation of strong ground motion, *Bull. Seism. Soc. Am*. 80, 1118–1143.

Uski, M., T. Hyvonen, A. Korja, and M. Airo (2003). Focal mechanisms of three earthquakes in Finland and their relation to surface faults, *Tectonophysics* 363, 141–157.

Zhao, L., and D. Helmberger (1991). Broadband modelling on a regional shield path, Harvard recording of the Saguenay earthquake, *Geophys. J. Int*. 105, 301–312

Zhao, L., and D. Helmberger (1993). Source retrieval from broadband regional seismograms: Hindu Kush region, *Phys. Earth and Planet. Inter*. 78, 69–95.

Zhu, L., and D. Helmberger (1997). Regional waveform calibration in the Pamir-Hindu Kush region, *J. Geophys. Res*. 102, 22799–22813.

Zonno, G., and R. Kind, (1984). Depth Determination of north Italian earthquakes using Grafenberg data, *Bull. Seism. Soc. Am.* 74, 1645–1659.